RSC Advances

This article can be cited before page numbers have been issued, to do this please use: R. Srivastava, B. Kaur and B. Satpati, *RSC Adv.*, 2015, DOI: 10.1039/C5RA19249H.

ROYAL SOCIETY OF CHEMISTRY

www.rsc.org/advances

View Article Online
DOI: 10.1039/C5RA19249H

A novel gold nanoparticles decorated nanocrystalline zeolite based electrochemical sensor for the nanomolar simultaneous detection of cysteine and glutathione

Balwinder Kaur[a], Rajendra Srivastava*[a], and Biswarup Satpati[b]

[a]*Department of Chemistry, Indian Institute of Technology Ropar, Rupnagar-140001, India*
[b]*Surface Physics and Material Science Division, Saha Institute of Nuclear Physics, 1/AF, Bidhannagar, Kolkata 700 064, India*

E-mail: rajendra@iitrpr.ac.in
Phone: +91-1881-242175; Fax: +91-1881-223395

View Article Online
DOI: 10.1039/C5RA19249H

Abstract

In this work, highly dispersed gold nanoparticles decorated nanocrystalline zeolite was synthesized by the electrostatic interaction between the functionalized gold nanoparticles and functionalized nanocrystalline zeolite. An electrochemical sensor based on gold nanoparticles decorated nanocrystalline zeolite was developed for the nanomolar simultaneous detection of cysteine and glutathione with high sensitivity, selectivity, and remarkably low detection limit. A wide linear range was obtained from 2 nM-800 μM and 3 nM-800 μM with a limit of detection of 0.3 nM and 0.6 nM for cysteine and glutathione, respectively. Analytical performance of the developed sensor was demonstrated in the determination of cysteine and glutathione in the commercial pharmaceutical preparations with satisfactory results even in the presence of several amino acids. The proposed methodology provides promising application in clinical diagnostic and drug analysis.

Keywords: Gold nanoparticles; Nanocrystalline zeolite; Electrocatalytic oxidation; Cysteine; Glutathione

View Article Online
DOI: 10.1039/C5RA19249H

Introduction

Human body is composed of large number of biomolecules (such as amino acids, proteins, carbohydrates, nucleic acids etc.) that govern the physiological function of the body. Abnormal concentration of these biomolecules is responsible for several diseases. Therefore, selective and sensitive detection of these biomolecules is very important in clinical diagnosis and pharmaceutical preparations. One such biomolecule is glutathione (GSH). GSH is synthesized in the body from the amino acids L-cysteine, L-glutamic acid, and glycine.[1] Cysteine (CySH) concentration is the rate limiting factor in glutathione biosynthesis because L-cysteine is relatively rare in food supplement and is usually synthesized in the human body.[1] Glutathione exists in reduced (GSH) and oxidized states (GSSG) in the body.[1] In the reduced state the –SH group of GSH can donate proton and electron to other unstable molecules such as reactive oxygen species. After donating proton and electron, two reactive glutathione molecules combine and form GSSG. GSH can be regenerated from GSSG by the enzyme glutathione reductase.[2] In healthy cells and tissues, more than 90% of total glutathione is in the reduced (GSH) form and less than 10% exists as GSSG.[3] An increased GSSG/GSH ratio is considered indicative of oxidative stress. Therefore, GSH acts as an important antioxidant and prevents damage to important cellular components caused by reactive oxygen species such as free radicals, peroxides, and heavy metals.[4] GSH is used in metabolic and biochemical reactions such as DNA synthesis and repair, protein synthesis, amino acid transport, and enzyme activation.[4] GSH also plays an important role in iron metabolism. Hence, every system in the body can be affected by the glutathione state especially the immune system, nervous system, and the lungs. GSH is also an essential antidote to the overdose of paracetamol (analgesic and antipyretic drug). The abnormal concentration of GSH in humans is directly related to various diseases such as Alzheimer's disease, Parkinson's disease, diabetes, macular degeneration, cancer and HIV/AIDS.[4-8] CySH is very important in GSH biosynthesis as discussed above and serves as an important amino acid in humans.[9-11] Since the GSH is related to the concentration of CySH, therefore, simultaneous detection of these biomolecules is very important in clinical diagnosis and pharmaceutical formulations. Since the -SH bond in GSH and CySH can be oxidized, so electrochemical technique can be employed for the detection and measurement of GSH and CySH. Moreover, the electrochemical methods are simple, cost effective, highly sensitive, and have capacity of being readily integrated with other techniques for multi-analysis. However, the

View Article Online
DOI: 10.1039/C5RA19249H

electrochemical oxidation of thiol group (-SH) at the conventional electrodes (gold, platinum, carbon) is very slow and requires very high potential (overpotential). In order to overcome these drawbacks, several chemically modified electrodes based on carbon, boron doped diamond, metal oxides, polymers, and layered double hydroxides with improved response have been developed.[9, 11-19] These modified electrodes were developed for the single determination of CySH or GSH. However, developing electrode materials for the simultaneous determination of these co-existing thiol containing biomolecules from their mixture solution with low limit of detection and high sensitivity is still a challenge. The present study is focused to achieve this motive.

Our research is mainly focused on the synthesis of nanocrystalline zeolites and explores their applications in electrocatalysis.[20-23] Through our recent studies we have shown that nanocrystalline zeolites remarkably improves the electrochemical sensing ability compared to the bulk zeolite.[24] For the electrochemical oxidation of GSH and CySH, some suitable redox active metal is also required. It is reported in the literature that gold can be used for the electrochemical oxidation of thiol group.[16, 25, 26] Hence, gold nanoparticles decorated nanocrystalline zeolite was synthesized and investigated in the electrochemical determination of CySH and GSH.

In this study, we present the synthesis of highly dispersed gold nanoparticles decorated nanocrystalline zeolite (AuNPs-Nano-ZSM-5) as an electrode material for the fabrication of electrochemical sensor for simultaneous determination of CySH and GSH. The developed AuNPs-Nano-ZSM-5 based sensor exhibited remarkably high activity, sensitivity, and selectivity. To the best of our knowledge, this is the first report which deals with the simultaneous electrochemical determination of CySH and GSH based on gold nanoparticles decorated Nano-ZSM-5 as an electrode material.

Experimental Section

Materials

All chemicals were of analytical reagent grade and used as received without further purification. Tetraethylorthosilicate (TEOS, 98%), tetrapropylammonium hydroxide (TPAOH), propyltriethoxy silane (PrTES, 97%), 3-aminopropyl trimethoxysilane, and gold (III) chloride trihydrate ($HAuCl_4.3H_2O$) were purchased from Sigma Aldrich, India. Sodium borohydride was obtained from Spectrochem Pvt. Ltd., India. Trisodium citrate was obtained from Loba Chemie

View Article Online
DOI: 10.1039/C5RA19249H

Pvt. Ltd., India. L-Cysteine was obtained from Himedia, India. Reduced glutathione was obtained from Sisco Research Laboratories Pvt. Ltd., India. Deionized water from Millipore Milli-Q system (Resistivity 18 MΩcm) was used in the electrochemical studies. Electrochemical measurements were performed in 0.1 M phosphate buffer (***Sorenson's buffer***) solution, which was prepared by mixing potassium monohydrogen phosphate (Na_2HPO_4) and potassium dihydrogen phosphate (NaH_2PO_4). All electrochemical experiments were performed in 0.1 M phosphate buffer solution (PBS) at pH 7.4.

Synthesis of AuNPs decorated Nano-ZSM-5 nanocomposite

Nanocrystalline ZSM-5 zeolite (Nano-ZSM-5) was prepared using molar composition TEOS/10 PrTES/2.5 Al_2O_3/3.3 Na_2O/25 TPAOH/2500 H_2O by following the reported procedure.[20] Propyl amine was then covalently anchored on the external surface of Nano-ZSM-5. Nano-ZSM-5 (2 g) and (3-aminopropyl)trimethoxysilane (1.43 g) were taken in 50 mL toluene and the reaction mixture was refluxed for 12 h. After the reaction, the reaction mixture was filtered and solid sample was washed with toluene followed by acetone and dried at 323 K for 24 h in oven to obtain propyl amine-functionalized Nano-ZSM-5 (hereafter represented as Nano-ZSM-5-Pr-NH_2).

For the synthesis of gold nanoparticles decorated Nano-ZSM-5 nanocomposite (hereafter represented as AuNPs(0.5%)-Nano-ZSM-5), Nano-ZSM-5-Pr-NH_2 (300 mg) was dispersed in ethanol (30 mL). Then acetic acid (3 mL) was added into it at ambient temperature to induce the positive charge on the surface of Nano-ZSM-5-Pr-NH_2. The solution was then sonicated at room temperature for 1 h. In another beaker, an aqueous solution (30 mL) containing $HAuCl_4$ (3 mg, 2.5 x 10^{-4} M) and trisodium citrate (2.24 mg, 2.5 x 10^{-4} M) was prepared and maintained at temperature 276-277 K. Then, cold $NaBH_4$ solution (0.9 mL, 0.1 M) was added with vigorous stirring to this $HAuCl_4$ solution at a temperature 276-277 K. The solution turned wine red immediately after the addition of $NaBH_4$, indicating the formation of gold nanoparticles. Finally, the solution of positively charged Nano-ZSM-5-Pr-NH_2 was added to the gold solution under sonication at room temperature and sonication was continued for further 30 min. The resulting product was centrifuged, washed with ethanol and water followed by drying at 333 K. AuNPs-Nano-ZSM-5 nanocomposites with different weight ratios (0.1, 1, and 3, denoted as AuNPs(0.1%)-Nano-ZSM-5, AuNPs(1%)-Nano-ZSM-5, and AuNPs(3%)-Nano-ZSM-5,

View Article Online
DOI: 10.1039/C5RA19249H

respectively) were also synthesized using the similar procedure with varying the amount of $HAuCl_4$.

Instrumentation

X-ray diffraction (XRD) patterns were recorded in the 2θ range of 5-80° with a scan speed of 2°/min on a PANalytical X'PERT PRO diffractometer, using Cu Kα radiation (λ=0.1542 nm, 40 kV, 40 mA) and a proportional counter detector. Nitrogen adsorption measurements were performed at 77 K by Quantachrome Instruments, Autosorb-IQ volumetric adsorption analyzer. Sample was out-gassed at 473 K for 3 h in the degas port of the adsorption apparatus. The specific surface area of zeolites was calculated from the adsorption data points obtained at P/P_0 between 0.05-0.3 using the Brunauer-Emmett-Teller (BET) equation. The pore diameter was estimated using the Barret–Joyner–Halenda (BJH) method. TEM investigations were carried out using FEI, Tecnai G^2 F30-ST microscope operated at 300 kV. High-angle annular dark field scanning transmission electron microscopy (HAADF-STEM) was used here using the same microscope, which was equipped with a scanning unit and a HAADF detector from Fischione (model 3000). The compositional analysis was performed using energy dispersive X-ray spectroscopy (EDS, EDAX Inc.) attachment on the Tecnai G^2 F30. The sample was dispersed in ethanol using ultrasonic bath, and dispersed sample was mounted on a carbon coated Cu grid, dried, and used for TEM measurement. Fourier transform infrared (FT-IR) spectra were recorded on a Bruker spectrophotometer in the region 600-4000 cm^{-1} (spectral resolution = 4 cm^{-1}; number of scans = 100). Thermogravimetric analysis (TGA) was performed on a TGA/DSC 1 $STAR^e$ SYSTEM from Mettler Toledo instrument with temperature increments of 10 K/min in air stream.

Electrode fabrication

Cyclic voltammetry (CV), differential pulse voltammetry (DPV), and chronoamperometry studies were performed using Potentiostat-Galvanostat BASi EPSILON, USA. A three-electrode electrochemical cell was employed with Ag/AgCl as the reference electrode (3M KCl), AuNPs-Nano-ZSM-5 mounted glassy carbon (3 mm diameter) as the working electrode and Pt foil as the counter electrode. Before modification, the glassy carbon electrode (GCE) was first polished to a mirror like surface with alumina slurry and then

View Article Online
DOI: 10.1039/C5RA19249H

ultrasonicated in ethanol and deionized water for 5 min, respectively. 10 µL aliquot of AuNPs-Nano-ZSM-5 suspension (a homogenous sonicated solution of 2 mg of AuNPs-Nano-ZSM-5, 10 µL of Nafion and 1 mL of deionized water) was placed onto the GCE surface. The electrode was dried in air leaving the material mounted onto the GC surface. For comparison, the other modified glassy carbon electrodes were also fabricated in a similar way. Electrochemical impedance spectroscopy (EIS) was performed using Autolab PGSTAT302N.

Real sample preparation

CySH syrup (Syp Amino Drip, Wockhardt (labeled value CySH = 5.6 mg/unit)) were obtained from Kailash Medical Store, Ropar, Punjab, India. Ropar. The CySH syrup also contained arginine, lysine, histidine, tyrosine, phenylalanine, tryptophan, methionine, glutamic acid, threonine, valine, alanine, proline, serine, and glycine along with CySH. 10 mL of 0.1 M stock solution of CySH was prepared using deionized water. Required amount of this solution was added to the electrochemical cell containing 10 mL of 0.1 M PBS (pH 7.4) for the determination of CySH. GSH injection (Injection Hepafresh, Macleods (labeled value GSH = 600 mg/injection)) was obtained from Kailash Medical Store, Ropar. 10 mL of 0.1 M stock solution of GSH injection was prepared using deionized water. Required amount of this solution was then added to the electrochemical cell containing 10 mL of 0.1 M PBS (pH 7.4) to record the DPV voltammogram.

Results and discussion

Mesoporous zeolites exhibit all the desired criteria to act as an ideal support materials. For the synthesis of AuNPs-Nano-ZSM-5, Nano-ZSM-5 was first surface functionalized with the propyl amine group (–Pr-NH_2). Nano-ZSM-5 possesses large external surface area and abundant surface silanol groups, therefore large amount of –Pr-NH_2 was incorporated on the surface of nanocrystalline zeolite. Then the –Pr-NH_2 group on Nano-ZSM-5 surface was protonated with acetic acid to induce the positive charge. Finally, freshly prepared citrate coated negatively charged gold nanoparticles were immobilized on Nano-ZSM-5 surface by electrostatic interactions as shown in Scheme 1.

View Article Online
DOI: 10.1039/C5RA19249H

Physico-chemical characterization

Nano-ZSM-5 exhibited XRD pattern corresponding to a highly crystalline MFI framework structure with high phase purity (Fig. 1a). MFI is a three letter code suggested by the International Zeolite Association for ZSM-5 framework topology. No change in the XRD pattern of Nano-ZSM-5-Pr-NH_2 was observed after the functionalization (Figure not shown), which confirms that the framework structure was not affected after the functionalization. XRD pattern of AuNPs(0.5%)-Nano-ZSM-5 did not exhibit any diffraction peak corresponding to AuNPs because of very low Au content in AuNPs(0.5%)-Nano-ZSM-5 (Fig. 1a). AuNPs(3%)-Nano-ZSM-5 exhibited the diffraction peaks corresponding to both, Nano-ZSM-5 phase and Au nanoparticles. Four diffraction peaks located at 2θ; 38.4, 44.5, 65, and 77.9°, which can be assigned to (111), (200), (220), and (311) planes of the fcc structure of gold (JCPDS, File No. 4-0784) were observed for AuNPs(3%)-Nano-ZSM-5 (Fig. 1a). This confirms the formation of AuNPs on Nano-ZSM-5. Textural properties of the zeolite materials were investigated using nitrogen adsorption-desorption measurements. Nano-ZSM-5 and Nano-ZSM-5-Pr-NH_2 exhibited type-IV isotherm similar to that of mesoporous materials (Fig. 1b). A sharp increase in the volume of N_2 adsorption in the region $0.4<P/P_0<0.9$ is characteristic of the capillary condensation within the intercrystalline mesopore void spaces. A pore size distribution in the range of 2–10 nm was obtained in the case of Nano-ZSM-5. Textural properties of zeolite materials are summarized in Table 1. The N_2-adsorption study confirms that the surface area and total pore volume decreased after the functionalization (Table 1). Nano-ZSM-5 has large external surface area with large number of surface silanol groups, which makes it ideal support for surface functionalization. Fourier transform infrared (FT-IR) spectroscopy was used to confirm the functionalization of -Pr-NH_2 on the surface of Nano-ZSM-5 (Details are provided in supporting information, Fig. S1). TGA analysis confirmed that 11 wt% organic group (-Pr-NH_2) was functionalized on Nano-ZSM-5 (Details are provided in the supporting information, Fig. S2). The amounts of Au incorporated in AuNPs(0.1%)-Nano-ZSM-5, AuNPs(0.5%)-Nano-ZSM-5, AuNPs(1%)-Nano-ZSM-5, and AuNPs(3%)-Nano-ZSM-5 were found to be 0.097, 0.485, 0.982, 2.810 wt %, respectively, which were estimated by atomic absorption spectrometer.

To obtain the in-depth information for AuNPs decorated Nano-ZSM-5, TEM investigation was made. Spheroid Nano-ZSM-5 aggregated morphology (having dimension of 300-500 nm) are actually composed of very small size nanocrystals of 10-20 nm as observed in

View Article Online
DOI: 10.1039/C5RA19249H

the high resolution TEM micrograph (Fig. S3, Supporting Information). Mesopores are created by the crystal packing of these zeolite nanocrystals. TEM investigations clearly show that highly dispersed Au nanoparticles were supported on the surface of Nano-ZSM-5 (Fig. 2a,b). HRTEM analysis confirmed that 3-5 nm spherical gold nanoparticles were formed on the surface of Nano-ZSM-5 (Fig. 2c). The HRTEM image in Fig. 2d clearly showing lattice fringes indicates the crystalline phase with a d-spacing of 2.33 Å. The measured d-spacing is very close to the (111) inter-planar spacing of *fcc* Au (2.35 Å). To confirm the presence of Si, Al, O, and Au elements in the material, EDX analysis was performed in STEM mode. EDX spectrum (Fig. 3b) from the high angle annular dark field (HAADF) image (Fig. 3a) clearly shows the incorporation of Au nanoparticles on Nano-ZSM-5 matrix.

Electrochemical characteristics of modified electrode

The electrochemical behavior of AuNPs(0.5%)-Nano-ZSM-5/GCE was investigated using CV. Fig. 4 shows the CVs at AuNPs(0.5%)-Nano-ZSM-5/GCE and bare GCE in 0.1 M PBS (pH 7.4) at a scan rate of 50 mV/s. The results show that no peak was observed at bare GCE. However, the CV at AuNPs(0.5%)-Nano-ZSM-5/GCE exhibited two distinct and sharp peaks corresponding to the formation of gold oxide during the anodic sweep and its reduction in the reverse scan ($2Au + 3H_2O \longleftrightarrow Au_2O_3 + 6H^+ + 6e^-$).[27, 28]

The electrochemical behavior of AuNPs(0.5%)-Nano-ZSM-5/GCE, Nano-ZSM-5/GCE and bare GCE was investigated using potassium ferricyanide as electrochemical probe by CV. Study was performed in 0.1 M KCl solution containing 10 mM $K_3[Fe(CN)_6]/K_4[Fe(CN)_6]$ at a scan rate of 10 mV/s at different modified electrodes and bare GCE. The CV of various modified electrodes and bare GCE exhibited a pair of redox peaks corresponding to $Fe(CN)_6^{3-/4-}$ redox couple (Fig. S4, Supporting Information). Fig. S4, Supporting Information shows that AuNPs(0.5%)-Nano-ZSM-5/GCE exhibited much higher peak current when compared to Nano-ZSM-5/GCE and bare GCE. This may be correlated to the synergistic contribution provided by electrochemically active gold nanoparticles and porous Nano-ZSM-5, which enhances the diffusion of analyte.

EIS is an effective technique to study the interfacial properties of surface modified electrodes (Fig. 5 and Fig. S5 & Fig. S6, Supporting Information). The Nyquist plot of impedance profile include a semicircle portion at higher frequencies corresponding to the

View Article Online
DOI: 10.1039/C5RA19249H

electron transfer-limited process and a linear part in the lower frequency range representing the diffusion limited process. The semicircle diameter in the impedance profile is a measure of the electron transfer-resistance (R_{et}). This resistance controls the electron-transfer kinetics of the redox couple at the electrode interface. Therefore, R_{et} can be used to describe the interfacial properties of the modified electrode. The impedance profile was recorded at three different conditions (Fig. 5 and Fig. S5 & Fig. S6, Supporting Information). Please note that R_{et} is highly depended on the applied frequency range (Compare Fig. 5 and Fig. S6, Supporting Information). It also depends on the electrolyte used in the study (KCl vs KNO_3) (Compare Fig. 5 and Fig. S5, Supporting Information). Mesoporous silica materials (eg SBA-15, MCM family etc) are insulator but zeolites are semiconductor. Zeolites are crystalline aluminosilicates build from TO_4 tetrahedra (T = Si, Al). Upon incorporation of Al into the silica framework, the +3 charge of the Al makes the framework negatively charged, and requires the presence of extra-framework cations (inorganic and organic cations) within the structure to keep the overall framework neutral. The extra-framework cations present in the zeolites have considerable mobility, which provides the conductivity in zeolites. In this study, we prepared Nano-ZSM-5 with silica/alumina ratio 20, thus it has sufficient number of Na^+ ions in its matrix. Due to the conducting nature of Nano-ZSM-5 (because of Na^+ ions present in the matrix), high surface area, and intercrystalline mesopores, diffusion of analyte is facilitated. Therefore, R_{et} for Nano-ZSM-5 was somewhat smaller than bare GCE. The modification of GCE with AuNPs(0.5%)-Nano-ZSM-5 displayed an almost straight line indicating negligible electron transfer resistance. Improved charge transfer rate at the electrode surface and diffusion controlled behavior observed in the EIS measurement with AuNPs(0.5%)-Nano-ZSM-5 modified electrode is important for the individual and simultaneous determination of analytes.

Voltammetric studies of cysteine and glutathione

The electrochemical behavior of CySH and GSH was investigated in detail at AuNPs(0.5%)-Nano-ZSM-5/GCE due to its high electrocatalytic activity. In order to mimic the physiological environment, pH 7.4 was chosen as the optimum pH value for all the experiments. Fig. 6 shows a comparison of CVs for CySH and GSH oxidation, individually, at AuNPs(0.5%)-Nano-ZSM-5/GCE and bare GCE in 0.1 M PBS (pH 7.4) at a scan rate of 50 mV/s. CV result shows that AuNPs(0.5%)-Nano-ZSM-5/GCE exhibited well defined and sharp oxidation peaks

View Article Online
DOI: 10.1039/C5RA19249H

for CySH and GSH with high current response (Fig. 6). However, bare GCE did not show any distinguishable oxidation peak for CySH and GSH. The poor voltammetric response at bare GCE may be attributed to the sluggish electron transfer kinetics. These results clearly show that the modification of GCE with AuNPs(0.5%)-Nano-ZSM-5 nanocomposite effectively accelerated the rate of electron transfer between the analytes and electrode. Therefore, the electrochemical behavior of CySH and GSH is considerably improved at AuNPs(0.5%)-Nano-ZSM-5/GCE. Based on the results obtained, it can be concluded that AuNPs(0.5%)-Nano-ZSM-5 have the ability to promote the electron transfer rate for CySH and GSH oxidation and have high electrocatalytic activity.

The effect of scan rate on the electrochemical oxidation of CySH and GSH was investigated using CV. Fig. S7a-b, Supporting Information shows the CVs at AuNPs(0.5%)-Nano-ZSM-5/GCE containing CySH and GSH in 0.1 M PBS (pH 7.4) at various scan rates (10-600 mV/s). The CV results for CySH and GSH show only an oxidation peak and no reduction peak was observed in the reverse scan which confirms that oxidation of CySH and GSH is an irreversible electrode process. Further, with increase in the scan rate, the oxidation peak current was increased for both CySH and GSH. The plot of the oxidation peak current against the square root of scan rate showed a linear relationship indicating a diffusion controlled process. The Semerano coefficient can be calculated from the logarithmic dependence of the electro-oxidation peak current on the scan rate ($\tan \alpha = \Delta \log I_p / \Delta \log \nu$, where I_p is the oxidation peak current and ν is the scan rate).[23] The plot of logarithm of anodic peak current vs. logarithm of scan rate provided a straight line with the linear regression equation $\log I_p = 0.452 \log \nu + 0.434$ ($R^2 = 0.987$) and $\log I_p = 0.527 \log \nu + 0.019$ ($R^2 = 0.996$), for CySH and GSH, respectively (Fig. S7c-d, Supporting Information). Slopes obtained from the linear behavior between the logarithm of anodic peak current vs. logarithm of scan rate for CySH and GSH were found to be 0.45 and 0.53, which are close to the theoretical value of 0.5 for a diffusion controlled process.

Chronoamperometry was used to calculate the kinetic parameters such as diffusion coefficient (D) and rate constant (k) for the electro-catalytic oxidation of CySH and GSH at AuNPs(0.5%)-Nano-ZSM-5/GCE (Fig. S8-S9, Supporting Information includes experimental details along with a brief discussion). The diffusion coefficients were found to be 3.1×10^{-5} and 1.4×10^{-5} cm^2/s for CySH and GSH, respectively. The rate constant values for electro-catalytic oxidation of CySH and GSH were found as 17.0×10^3 and 3.2×10^3 1/s M, respectively. This

View Article Online
DOI: 10.1039/C5RA19249H

chronoamperometric data indicates that the electrochemical reaction rate for CySH and GSH at AuNPs(0.5%)-Nano-ZSM-5/GCE is fast.

The total number of electrons (n) involved in the electrochemical oxidation of CySH and GSH at AuNPs(0.5%)-Nano-ZSM-5/GCE can be calculated from the plot of oxidation peak currents against the square root of scan rate according to the following equation for a totally irreversible diffusion-controlled process.[29-31] The total number of electrons was calculated to be 1.8 and 2.1 for CySH and GSH, respectively. Hence, a total of 2 electrons were involved in the electrochemical oxidation of CySH and GSH.

$$I_p = 3.01 \times 10^5 n[n_\alpha(1-\alpha)]^{1/2} ACD^{1/2} \nu^{1/2}$$

Where I_p is the peak current (A), n_α is the number of electrons in rate determining step, α is charge transfer coefficient, A is electrode surface area (0.07 cm^2), C is the bulk concentration of analyte (mol/cm^3), D is the diffusion coefficient of analyte (3.1×10^{-5} cm^2/s for CySH and 1.4×10^{-5} cm^2/s for GSH; obtained from the chronoamperometric study), and ν is the scan rate (V/s). The charge transfer coefficient between the analyte (CySH and GSH) and AuNPs(0.5%)-Nano-ZSM-5/GCE was obtained from Tafel plot using the rising part of the current-voltage plot (Fig. S10, Supporting Information). A slope of 8.31 V^{-1} and 8.12 V^{-1} was obtained for CySH and GSH, respectively. Assuming one electron transfer in the rate-determining step ($n_\alpha = 1$), charge transfer coefficient (α) was calculated as 0.51 and 0.53 for CySH and GSH, respectively, according to the equation $b = n_\alpha(1- \alpha) F/2.3 RT$, where b is slope of tafel plot. Based on the above results and the literature reports, the mechanism for the electrochemical oxidation of CySH and GSH at AuNPs(0.5%)-Nano-ZSM-5/GCE is proposed (Scheme 2).[12, 15, 32]

Individual electro-catalytic oxidation of CySH and GSH

The individual electrocatalytic oxidation of CySH and GSH at AuNPs(0.5%)-Nano-ZSM-5/GCE was carried out using DPV in 0.1 M PBS (pH 7.4) at a scan rate 20 mV/s (Fig. 7). The DPV results show that both the analytes were oxidized with well-defined and distinguishable sharp oxidation peaks with peak potentials at 334 and 573 mV for CySH and GSH, respectively, at AuNPs(0.5%)-Nano-ZSM-5/GCE (Fig. 7). The peak currents were found to increase linearly with the increase in the concentration of CySH and GSH in the

View Article Online
DOI: 10.1039/C5RA19249H

electrochemical cell. A linear dynamic range from 1 nM to 1000 µM with a calibration equation of $I_{CySH}(\mu A) = 9.788 + 0.083\ C_{CySH}(\mu M)$ (R^2= 0.997) was obtained for CySH (Fig. 7a, inset). A linear calibration for GSH was found to be in the range of 2 nM to 1000 µM, with a calibration equation of $I_{GSH}(\mu A) = 8.309 + 0.061\ C_{GSH}\ (\mu M)$ (R^2= 0.995) (Fig. 7b, inset). The limit of detection (S/N = 3) was found to be 0.2 nM and 0.5 nM for CySH and GSH, respectively.

Simultaneous electrochemical determination of CySH and GSH

DPV was employed for the simultaneous determination of CySH and GSH at AuNPs(0.5%)-Nano-ZSM-5/GCE in 0.1 M PBS (pH 7.4) at a scan rate 20 mV/s (Fig. 8). Fig. 8 shows that two distinguished and sharp anodic peaks at potentials 334 and 573 mV corresponding to the oxidation of CySH and GSH were obtained in the simultaneous determination. These peak potentials matched well with their individual anodic peak potentials as discussed in the above section. The voltammograms for the binary mixture were well separated from each other with a potential difference of $\Delta E_{CySH-GSH}$ = 239 mV. This peak potential difference is large enough for the simultaneous determination of CySH and GSH from their binary solution. A significant increase in the oxidation peak current was observed for both the analytes with the increase in concentration of analytes in the electrochemical cell. The anodic peak current obtained was found to be linearly dependent on the concentration of analytes in the range of 2 nM to 800 µM (R^2= 0.998) for CySH and 3 nM to 800 µM (R^2= 0.998) for GSH with the sensitivity of 1.4 and 1.1 µA/ µM cm^2 and the limit of detection (S/N = 3) of 0.3 nM and 0.6 nM for CySH and GSH, respectively, (Fig. 8, inset). These results demonstrate that AuNPs(0.5%)-Nano-ZSM-5/GCE exhibited excellent electro-catalytic activity toward the simultaneous determination of CySH and GSH.

A comparison for the electrochemical oxidation of CySH and GSH at gold nanoparticles decorated Nano-ZSM-5 modified GCE with different weight ratios is provided in Fig. S11, Supporting Information. Fig. S11, Supporting Information shows that with increase in the amount of AuNPs on Nano-ZSM-5 support, the electrochemical activity was increased. This shows that higher loading of AuNPs in nanocomposite material is better for the high electrocatalytic activity. However, with further increase in AuNPs content (after AuNPs(0.5%)), the electrocatalytic activity was decreased. These results clearly show that the highly dispersed AuNPs on the surface of Nano-ZSM-5 enhanced the accessibility of analytes to the active sites

View Article Online
DOI: 10.1039/C5RA19249H

and improved the electrocatalytic activity of material. With further increase in the Au content, less dispersed AuNPs with larger size were formed that resulted in the lower current response. These results show that optimum loading and high dispersion of AuNPs on Nano-ZSM-5 surface is required to achieve high electrocatalytic activity. Therefore, AuNPs(0.5%)-Nano-ZSM-5/GCE was chosen for the determination of CySH and GSH. A comparison of AuNPs(0.5%)-Nano-ZSM-5/GCE, Nano-ZSM-5/GCE, and bare GCE in the simultaneous determination of CySH and GSH is shown in (Fig. 9 and Fig. S12, Supporting Information). Bare GCE did not exhibit any oxidation peak in the simultaneous determination of CySH and GSH (Fig. S12, Supporting Information). Nano-ZSM-5/GCE exhibited oxidation peaks for CySH and GSH but with very low current response when compared to AuNPs(0.5%)-Nano-ZSM-5/GCE (Fig. S12, Supporting Information). This further confirms that Au nanoparticles play an important role in the electrochemical oxidation of CySH and GSH and have electrocatalytic effect in the oxidation of CySH and GSH. The remarkable high activity of AuNPs(0.5%)-Nano-ZSM-5/GCE can be attributed to the synergistic contribution provided by highly dispersed AuNPs and high surface area of Nano-ZSM-5. The inter-crystalline mesoporosity in Nano-ZSM-5 provides an efficient transport path for reactant/product molecules because of the short diffusion length. The comparison of results shown in this paper with literature reports are provided in Table S1, Supporting Information. It is clear from Table S1, Supporting Information, that the proposed sensor is able to detect CySH and GSH simultaneously with a wide linear range and remarkably low limit of detection when compared to literature reports.

Reproducibility, stability, and anti-interference property of the sensor

The reproducibility, repeatability, and long term stability of the developed sensor were evaluated in the sensing studies. Five, AuNPs(0.5%)-Nano-ZSM-5/GCE were constructed and their current response to 1 μM concentration of CySH and GSH was investigated (Fig. S13a, Supporting Information). The relative standard deviation (RSD) was found to be 1.3 % and 1.5 % for CySH and GSH, respectively, confirming that the fabrication method was highly reproducible. The stability of AuNPs(0.5%)-Nano-ZSM-5/GCE was examined by recording repetitive CVs for 50 scans in PBS (pH 7.4) at a scan rate 50 mV/s (Fig. S14 and Fig. S15, Supporting Information). No obvious change in the peak current was observed after 50 cycles, which confirms that AuNPs(0.5%)-Nano-ZSM-5/GCE is highly stable. The long term stability of

View Article Online
DOI: 10.1039/C5RA19249H

the sensor was evaluated by measuring its sensitivity toward 1 μM concentration of CySH and GSH for 30 days (Fig. S13b, Supporting Information). The sensor was stored in refrigerator at 278 K and its sensitivity was tested at the interval of 5 days. Prior to each measurement, electrode was washed with 0.1 M PBS and repetitive CV were run in blank 0.1 M PBS (pH 7.4). The results confirmed that the DPV response of the electrode to the same concentration of CySH and GSH remained almost same with RSD 2.1 % and 2.8 % for CySH and GSH respectively, indicating that the modified electrode has excellent stability. The selectivity of AuNPs(0.5%)-Nano-ZSM-5/GCE toward simultaneous determination of CySH and GSH was investigated in the presence of various interfering agents. The DPV responses are shown in Fig. S16, Supporting Information. No obvious deviation upon the addition of very high concentration of interferents (500 times excess) was observed. The results showed that other L-amino acids such as alanine, glycine, arginine, histidine, phenylalanine, proline, tyrosine, valine, tryptophan, glutamic acid, serine, threonine, and methionine had no effect on the peak currents for the oxidation of CySH and GSH. The presence of other common interferents such as glucose, ascorbic acid, dopamine, and uric acid did not show any change in the peak current response confirming that no interference for these common species occurred. These results confirmed that AuNPs(0.5%)-Nano-ZSM-5/GCE is highly selective for the determination of CySH and GSH.

Determination of CySH and GSH in pharmaceutical preparations

In order to show the analytical application of the developed sensor; experiments were performed to determine the concentration of CySH and GSH in pharmaceutical preparations and the results are listed in Table 2. The standard addition method was used by spiking with standard solution of CySH and GSH. The values of recovery were in the range from 99.4 to 100.6 %, suggesting the accuracy of AuNPs(0.5%)-Nano-ZSM-5 based sensor. These results confirm that proposed sensor is reliable and sensitive enough for the determination of CySH and GSH in real pharmaceutical samples even in the presence of other amino acids (see the details in the experimental section).

Conclusions

In summary, gold nanoparticles decorated nanocrystalline zeolite was synthesized. Transmission electron microscopy investigations confirmed that highly dispersed gold

View Article Online
DOI: 10.1039/C5RA19249H

nanoparticles (particle size 3-5 nm) were supported on nanocrystalline zeolite Nano-ZSM-5. An electrochemical sensor based on gold nanoparticles supported Nano-ZSM-5 modified glassy carbon electrode was fabricated for the simultaneous determination of thiol containing bio-molecules cysteine and glutathione. The results demonstrate that the developed sensor exhibited high electro-catalytic activity, sensitivity, selectivity, and stability in the detection of cysteine and glutathione. The high activity of AuNPs(0.5%)-Nano-ZSM-5 can be attributed to the synergistic contribution provided by highly dispersed Au nanoparticles, large surface area and mesopores of Nano-ZSM-5 support. The analytical performance of the developed sensor was extended in the determination of these biomolecules in pharmaceutical preparations with satisfactory results. The high sensitivity and selectivity together with very low limit of detection of the proposed sensor makes it a promising candidate for the determination of very low amount of cysteine and glutathione in pharmaceutical preparations. The proposed methodology is simple, rapid and provides a potentially new analytical platform for the sensitive and selective analysis of thiols.

Acknowledgements

Authors thank Department of Science and Technology, New Delhi for financial assistance (DST grant SB/S1/PC-91/2012). BK is grateful to CSIR, New Delhi for SRF fellowship. Authors are also thankful to Director IIT Ropar for his constant encouragement.

Supporting Information

The supporting information contains additional diffusion coefficient and rate constant calculation and results and discussion as noted in text.

View Article Online
DOI: 10.1039/C5RA19249H

References

1. A. Pompella, A. Visvikis, A. Paolicchi, V. De Tata and A. F. Casini, *Biochem. Pharmacol.*, 2003, **66**, 1499-1503.
2. N. Couto, N. Malys, S. J. Gaskell and J. Barber, *J. Proteome Res.*, 2013, **12**, 2885-2894.
3. A. Pastore, F. Piemonte, M. Locatelli, R. A. Lo, L. M. Gaeta, G. Tozzi and G. Federici, *Clin. Chem.*, 2001, **47**, 1467-1469.
4. J. C. Harfield, C. Batchelor-McAuley and R. G. Compton, *Analyst*, 2012, **137**, 2285-2296.
5. W. W. Huber and W. Parzefall, *Curr. Opin. Pharmacol.*, 2007, **7**, 404-409.
6. D. J. Naisbitt, F. J. Vilar, A. C. Stalford, E. G. Wilkins, M. Pirmohamed and B. K. Park, *AIDS Res. Hum. Retroviruses*, 2000, **16**, 1929-1938.
7. M. M. Monick, L. Samavati, N. S. Butler, M. Mohning, L. S. Powers, T. Yarovinsky, D. R. Spitz and G. W. Hunninghake, *J. Immunol.*, 2003, **171**, 5107-5115.
8. S. El Sayed, C. Giménez, E. Aznar, R. Martínez-Máñez, F. Sancenón and M. Licchelli, *Org. Biomol. Chem.*, 2015, **13**, 1017-1021.
9. C. Xiao, J. Chen, B. Liu, X. Chu, L. Wu and S. Yao, *PCCP*, 2011, **13**, 1568-1574.
10. W. Wang, O. Rusin, X. Xu, K. K. Kim, J. O. Escobedo, S. O. Fakayode, K. A. Fletcher, M. Lowry, C. M. Schowalter and C. M. Lawrence, *J. Am. Chem. Soc.*, 2005, **127**, 15949-15958.
11. M. Ahmad, C. Pan and J. Zhu, *J. Mater. Chem.*, 2010, **20**, 7169-7174.
12. R. Moradi, S. Sebt, H. Karimi-Maleh, R. Sadeghi, F. Karimi, A. Bahari and H. Arabi, *PCCP*, 2013, **15**, 5888-5897.
13. L. Pei, Y. Pei, Y. Xie, C. Fan and H. Yu, *CrystEngComm*, 2013, **15**, 1729-1738.
14. Y. Dong, Q. Sheng, J. Zheng and H. Tang, *Anal. Methods*, 2014, **6**, 8598-8603.
15. Y. Wang, W. Peng, L. Liu, F. Gao and M. Li, *Electrochim. Acta*, 2012, **70**, 193-198.
16. S. Ge, M. Yan, J. Lu, M. Zhang, F. Yu, J. Yu, X. Song and S. Yu, *Biosens. Bioelectron.*, 2012, **31**, 49-54.
17. Y.-P. Hsiao, W.-Y. Su, J.-R. Cheng and S.-H. Cheng, *Electrochim. Acta*, 2011, **56**, 6887-6895.
18. H. Pang, Y. Shi, J. Du, Y. Ma, G. Li, J. Chen, J. Zhang, H. Zheng and B. Yuan, *Electrochim. Acta*, 2012, **85**, 256-262.

View Article Online
DOI: 10.1039/C5RA19249H

19. Y. Hou, J. C. Ndamanisha, L.-p. Guo, X.-j. Peng and J. Bai, *Electrochim. Acta*, 2009, **54**, 6166-6171.
20. B. Kaur, M. U. Anu Prathap and R. Srivastava, *ChemPlusChem*, 2012, **77**, 1119-1127.
21. B. Kaur, B. Satpati and R. Srivastava, *New J. Chem.*, 2015, **39**, 1115-1124.
22. B. Kaur and R. Srivastava, *Electrochim. Acta*, 2014, **133**, 428-439.
23. B. Kaur and R. Srivastava, *Sens. Actuators, B: Chem.*, 2015, **211**, 476-488.
24. B. Kaur, R. Srivastava and B. Satpati, *ChemElectroChem*, 2015, **2**, 1164-1173.
25. F. d. A. dos Santos Silva, M. G. A. da Silva, P. R. Lima, M. R. Meneghetti, L. T. Kubota and M. O. F. Goulart, *Biosens. Bioelectron.*, 2013, **50**, 202-209.
26. H. He, J. Du, Y. Hu, J. Ru and X. Lu, *Talanta*, 2013, **115**, 381-385.
27. U. Oesch and J. Janata, *Electrochim. Acta*, 1983, **28**, 1237-1246.
28. R. Gupta and V. Ganesan, *Sens. Actuators, B: Chem.*, 2015, **219**, 139-145.
29. H. R. Zare and N. Nasirizadeh, *Electrochim. Acta*, 2007, **52**, 4153-4160.
30. H. Zare, N. Nasirizadeh and M. M. Ardakani, *J. Electroanal. Chem.*, 2005, **577**, 25-33.
31. M. U. Anu Prathap, V. Anuraj, B. Satpati and R. Srivastava, *J. Hazard. Mater.*, 2013, **262**, 766-774.
32. M. R. Shahmiri, A. Bahari, H. Karimi-Maleh, R. Hosseinzadeh and N. Mirnia, *Sens. Actuators, B: Chem.*, 2013, **177**, 70-77.

View Article Online
DOI: 10.1039/C5RA19249H

Figures, Tables and Scheme captions

Figures

Fig. 1 (a) XRD patterns of Nano-ZSM-5, AuNPs(0.5%)-Nano-ZSM-5, and AuNPs(3%)-Nano-ZSM-5; and (b) N_2-adsorption isotherms of Nano-ZSM-5 and Nano-ZSM-5-Pr-NH_2. Inset shows the pore size distribution.

Fig. 2 (a) Low magnification TEM image, (b) High magnification TEM image, (c) High magnification TEM image showing gold nanoparticles decorated on Nano-ZSM-5 surface, (d) HRTEM image showing single crystal structure of one AuNP shown in (c).

Fig. 3 (a) STEM-HAADF image of gold nanoparticles decorated on Nano-ZSM-5, (b) EDX spectrum from a rectangular region in (a).

Fig. 4 CV response of AuNPs(0.5%)-Nano-ZSM-5/GCE in 0.1 M PBS (pH 7.4) at a scan rate of 50 mV/s. Inset shows the CV response at bare GCE in 0.1 M PBS (pH 7.4) at a scan rate of 50 mV/s.

Fig. 5 Nyquist plots of impedance profiles at AuNPs(0.5%)-Nano-ZSM-5/GCE, Nano-ZSM-5/GCE, and bare GCE in 0.1 M KNO_3 solution containing 10 mM $[Fe(CN)_6]^{3-/4-}$ over the frequency range from 0.1 Hz to 10^5 Hz at an applied potential of 0.3 V.

Fig. 6 Comparison of CVs in a 0.1 M PBS (pH 7.4) containing (a) CySH (10 μM) and (b) GSH (10 μM) at AuNPs(0.5%)-Nano-ZSM-5/GCE and bare GCE at a scan rate of 50 mV/s.

Fig. 7 DPVs at AuNPs(0.5%)-Nano-ZSM-5/GCE in 0.1 M PBS (pH 7.4) by varying the concentrations of (a) CySH and (b) GSH. DPV parameters were selected as: pulse amplitude: 50 mV, pulse width: 50 ms, scan rate: 20 mV/s. Inset shows the calibration plot.

Fig. 8 DPVs of the binary mixture containing varying concentrations of CySH and GSH at AuNPs(0.5%)-Nano-ZSM-5/GCE in 0.1 M PBS (pH 7.4). DPV parameters were selected as: pulse amplitude: 50 mV, pulse width: 50 ms, scan rate: 20 mV/s. Inset shows the calibration plot for CySH and GSH.

Fig. 9 Comparison of the sensitivity for CySH and GSH electro-oxidation at AuNPs(0.5%)-Nano-ZSM-5/GCE and Nano-ZSM-5/GCE .

View Article Online
DOI: 10.1039/C5RA19249H

Table

Scheme

View Article Online
DOI: 10.1039/C5RA19249H

Table 1

S.No.	Sample	Total surface area S_{BET} (m^2/g)	External surface area (m^2/g)	Total pore volume (cm^3/g)
1.	Nano-ZSM-5	548	365	0.58
2.	Nano-ZSM-5-Pr-NH_2	335	164	0.33

View Article Online
DOI: 10.1039/C5RA19249H

Table 2

S. No.	Sample	Spiking (nM)	Original (nM)	Detected (nM)	RSD (%)[a]	Recovery (%)
1.	CySH Syrup	-	500	502	2.4	100.4
2.	CySH Syrup	100	500	599	2.6	99.8
3.	CySH Syrup	100	600	703	3.2	100.5
4.	CySH Syrup	100	700	801	1.9	100.1
5.	GSH Injection	-	500	497	2.7	99.4
6.	GSH Injection	100	500	603	2.9	100.6
7.	GSH Injection	100	600	702	1.8	100.3
8.	GSH Injection	100	700	804	2.6	100.6

[a]Average value of five determinations.

View Article Online
DOI: 10.1039/C5RA19249H

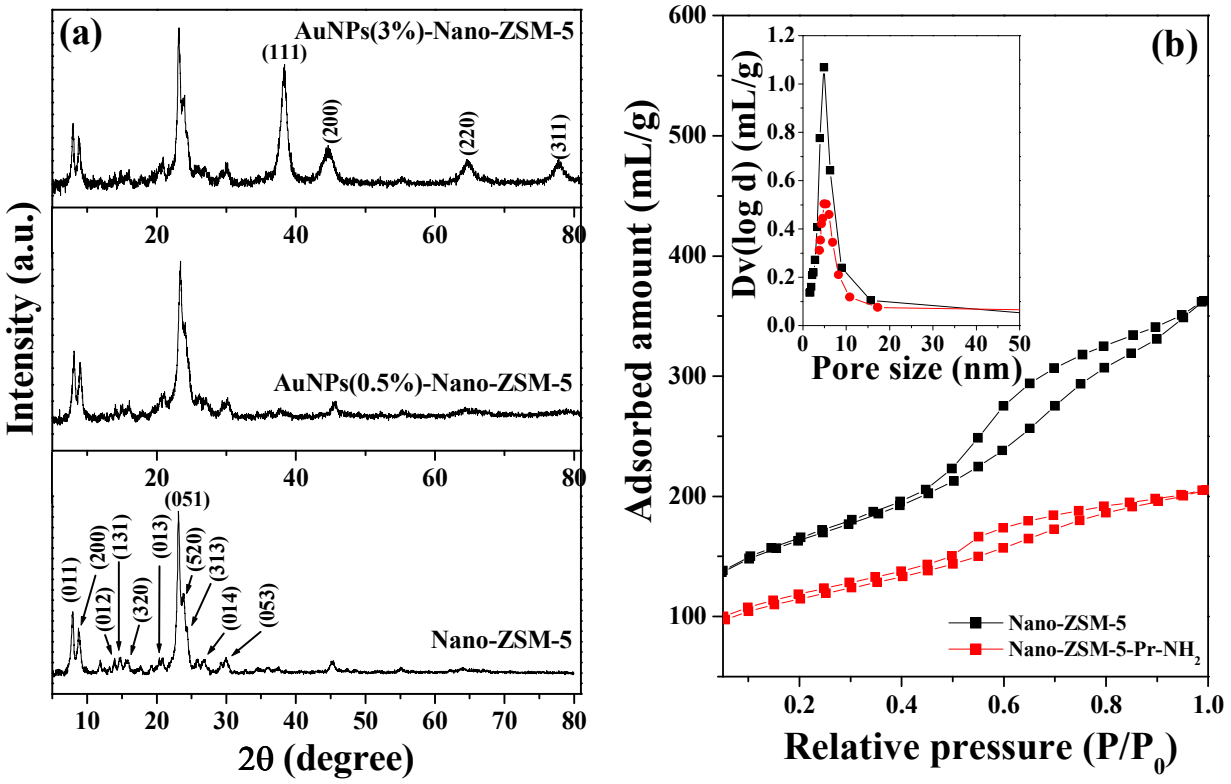

Fig. 1

View Article Online
DOI: 10.1039/C5RA19249H

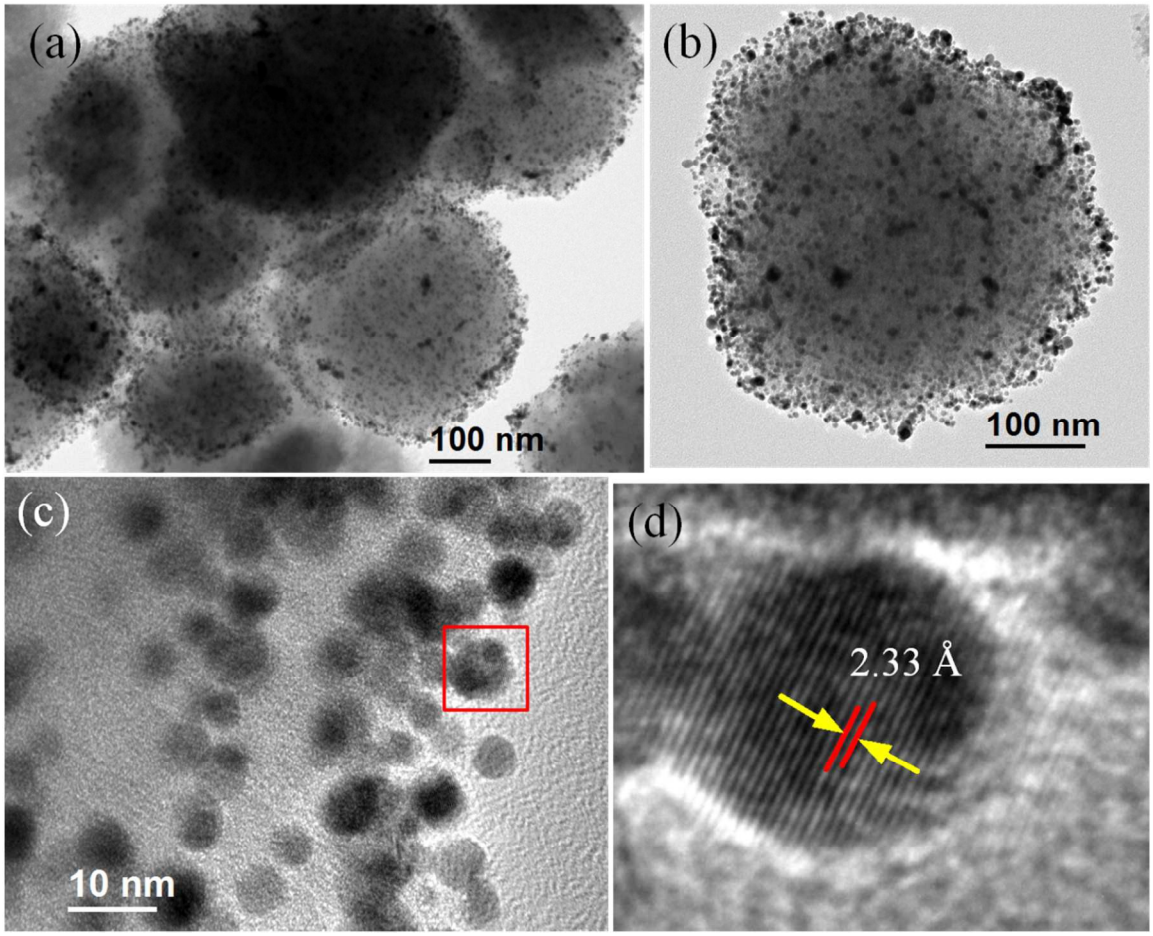

Fig. 2

View Article Online
DOI: 10.1039/C5RA19249H

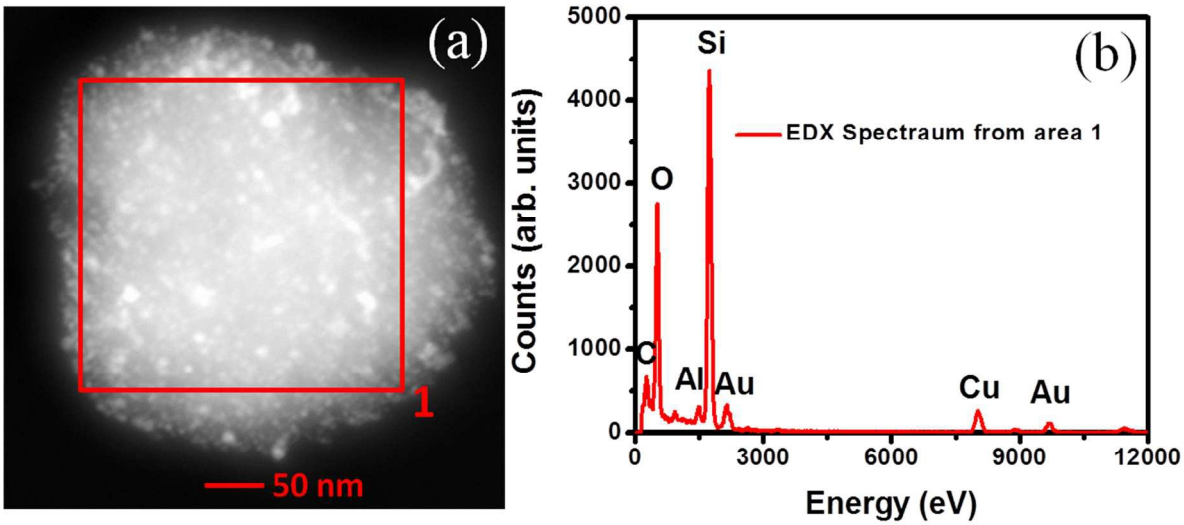

Fig. 3

View Article Online
DOI: 10.1039/C5RA19249H

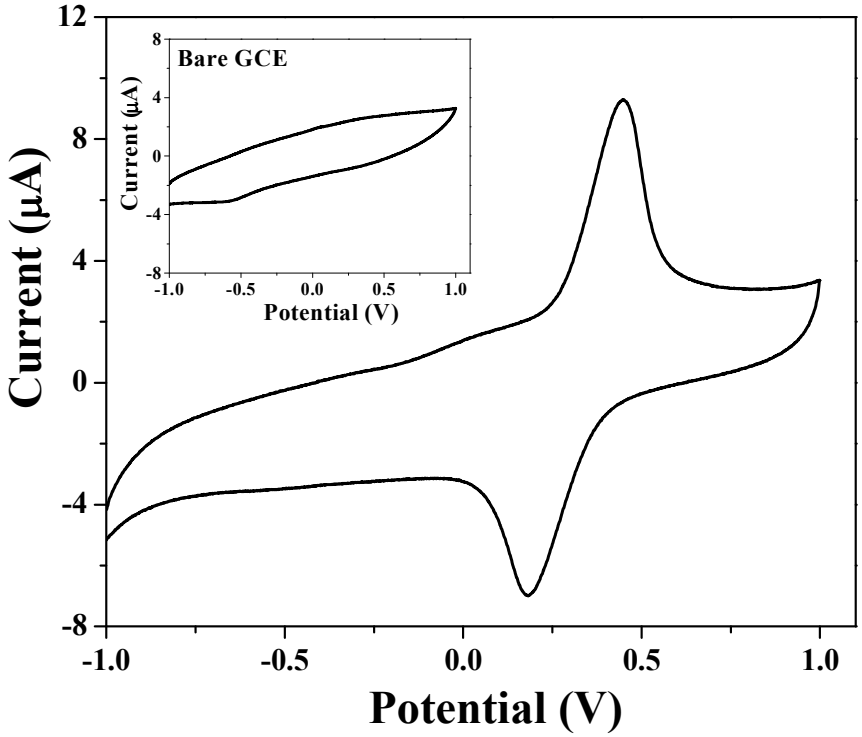

Fig. 4

View Article Online
DOI: 10.1039/C5RA19249H

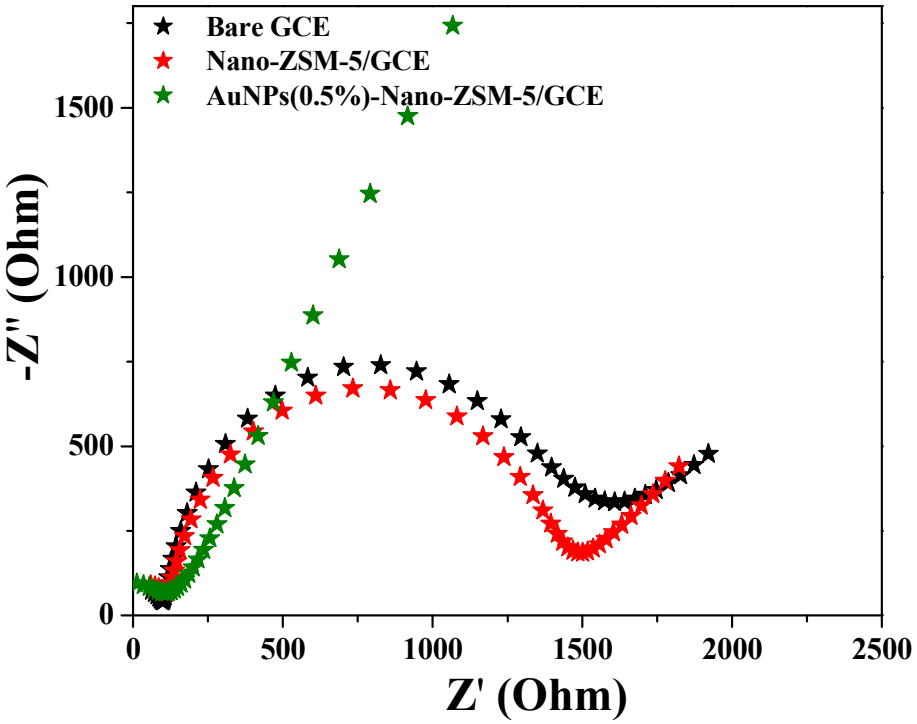

Fig. 5

View Article Online
DOI: 10.1039/C5RA19249H

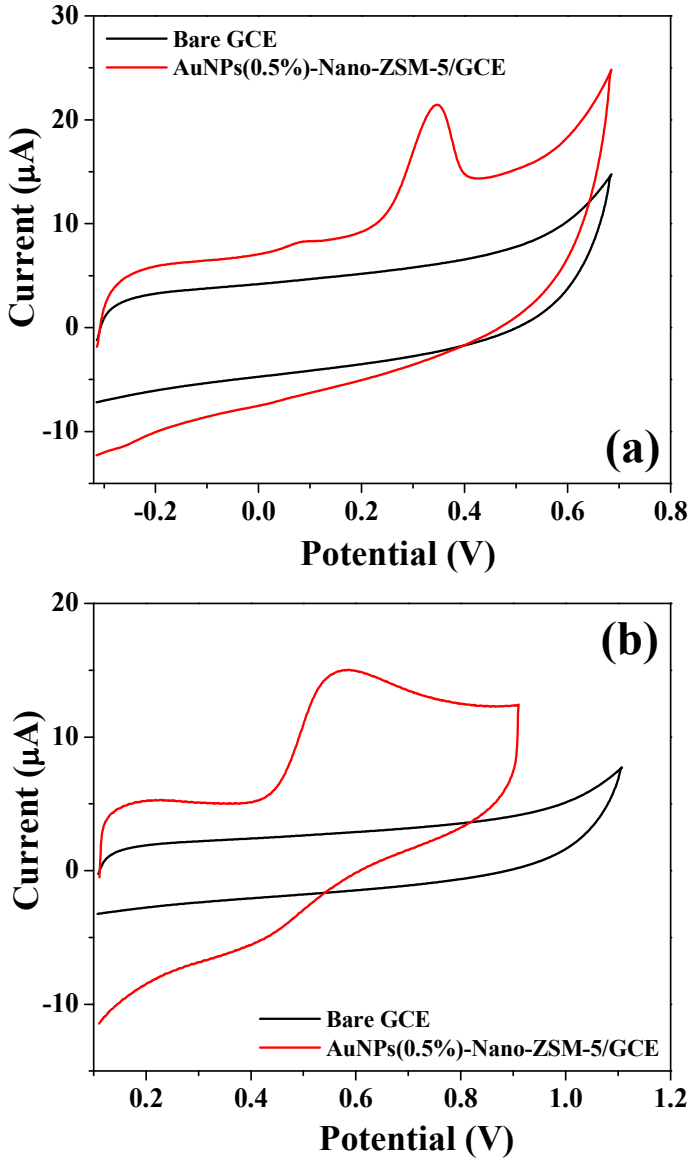

Fig. 6

View Article Online
DOI: 10.1039/C5RA19249H

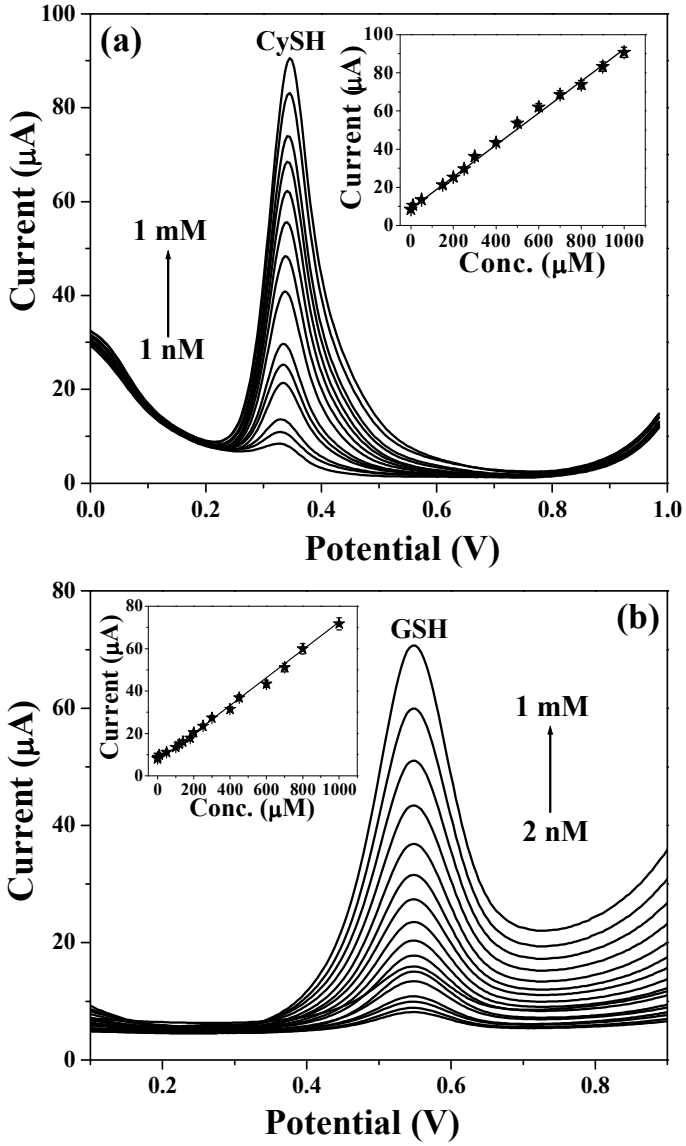

Fig. 7

View Article Online
DOI: 10.1039/C5RA19249H

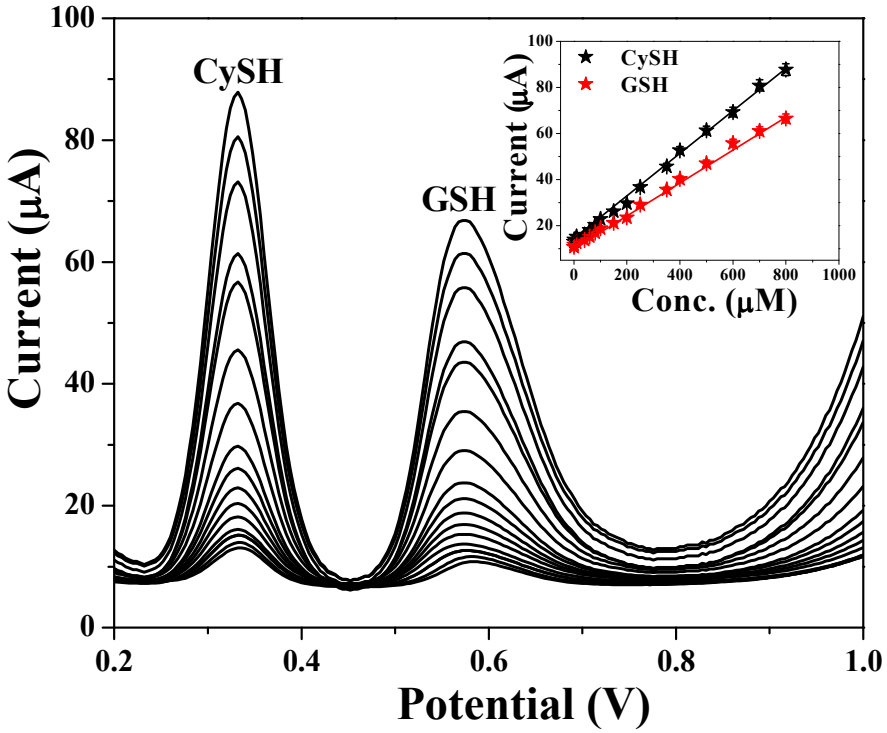

Fig. 8

View Article Online
DOI: 10.1039/C5RA19249H

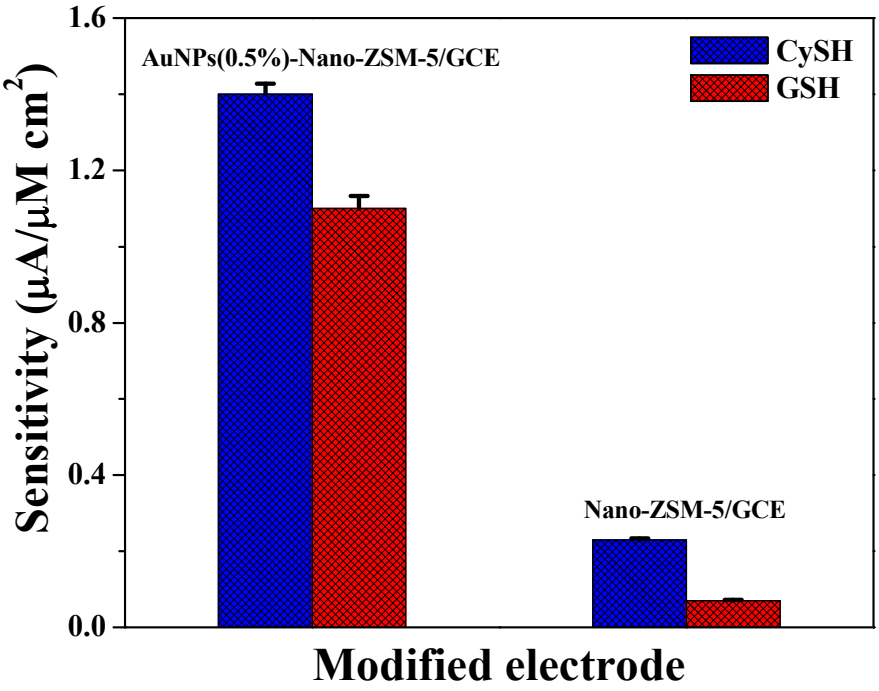

Fig. 9

View Article Online
DOI: 10.1039/C5RA19249H

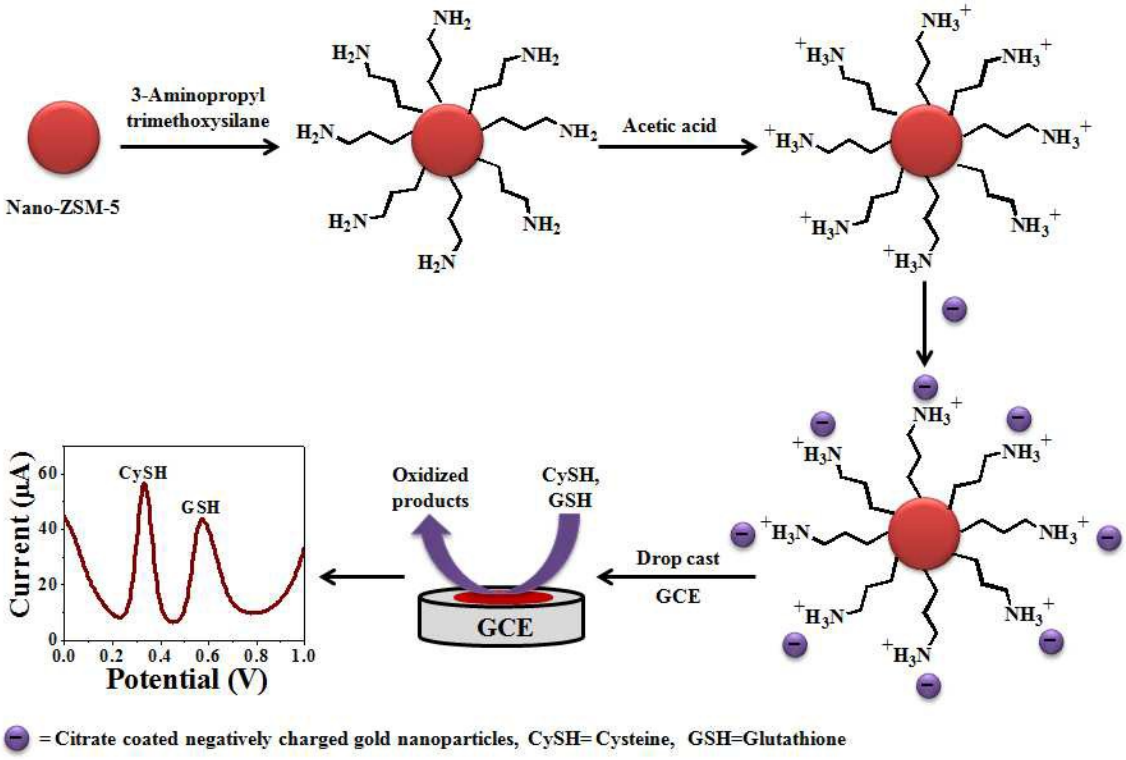

Scheme 1

View Article Online
DOI: 10.1039/C5RA19249H

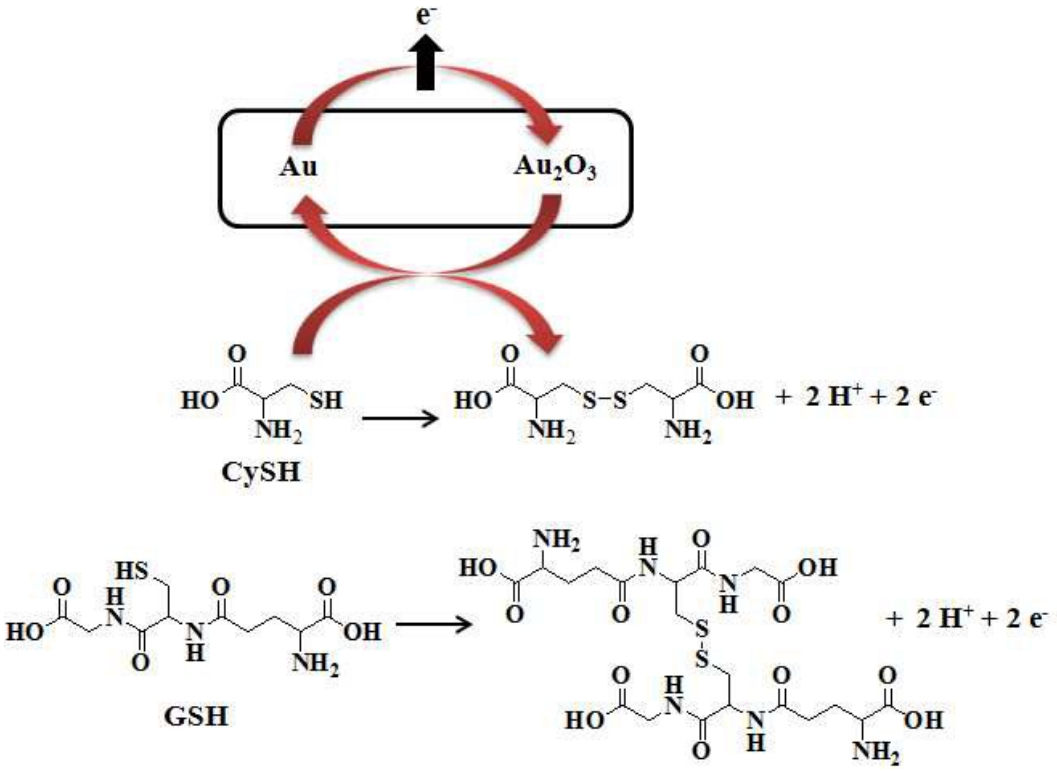

Scheme 2

View Article Online
DOI: 10.1039/C5RA19249H

Graphical Abstract

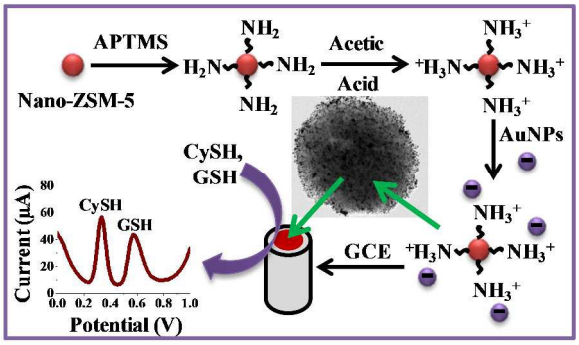

High electrocatalytic activity of the sensor can be attributed to the highly dispersed gold nanoparticles on nanocrystalline zeolite matrix.